

MultiLoc: Multi-view Guided Relative Pose Regression for Fast and Robust Visual Re-Localization

Nobel Dang and Bing Li*

Clemson University, SC, USA

Abstract. Relative Pose Regression (RPR) generalizes well to unseen environments, but its performance is often limited due to pairwise and local spatial views. To this end, we propose MultiLoc, a novel multi-view guided RPR model trained at scale, equipping relative pose regression with globally consistent spatial and geometric understanding. Specifically, our method jointly fuses multiple reference views and their associated camera poses in a single forward pass, enabling accurate zero-shot pose estimation with real-time efficiency. To reliably supply informative context, we further propose a co-visibility-driven retrieval strategy for geometrically relevant reference view selection. MultiLoc establishes a new benchmark in visual re-localization, consistently outperforming existing state-of-the-art (SOTA) relative pose regression (RPR) methods across diverse datasets, including WaySpots, Cambridge Landmarks, and Indoor6. Furthermore, MultiLoc’s pose regressor exhibits SOTA performance in relative pose estimation, surpassing RPR, feature matching and non-regression-based techniques on the MegaDepth-1500, ScanNet-1500, and ACID benchmarks. These results demonstrate robust domain generalization of MultiLoc across indoor, outdoor and natural environments. Code will be made publicly available.

Keywords: Visual Re-Localization · Pose Regression · Multi-view

1 Introduction

Visual Re-localization aims to understand the current position and orientation of an agent situated in a known environment based solely on the visual observations. The said known environment typically encapsulates images of a scene, also known as reference images, along with its’ camera poses. These reference poses—typically derived from Structure from Motion (SfM), high-precision 3D scanners, or geo-tagged—provide a global reset that eliminates the drift inherent in IMUs, wheel odometry, and incremental SLAM systems. Beyond drift rectification, visual re-localization also serves as a robust mechanism for estimating the real-time camera pose with high accuracy. By enabling system initialization, loop closure and accurate pose estimation especially in GNSS-denied environments like indoor, off-road and urban, visual re-localization facilitates centimeter-level

* DISTRIBUTION STATEMENT A. Approved for public release; distribution is unlimited. OPSEC # 10390

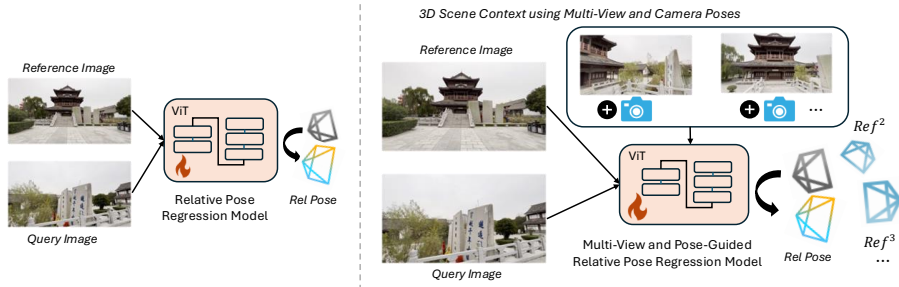


Fig. 1: Illustration of improving pose regression through scene context grounding. Estimating camera pose from image pairs can be erroneous especially when there is little-to-no co-visibility between frames. To solve this, our proposed method (right) moves beyond the standard visual-only approach (left). By incorporating multi-view images and existing pose data, we create a sub-scene context that grounds the query image. This additional spatial information provides the necessary cues to stabilize pose estimation even when direct co-visibility is low.

precision and long-term autonomy. Therefore, many works focus on visual re-localization as a crucial task for autonomous driving [30], robot navigation [45], augmented reality (AR) [10] and other robotic applications.

Traditionally, structure based methods [39,40,46] are employed that typically require creating an explicit map representation of the environment and then establishing 2D-3D correspondences between query image and the map followed by geometric optimization and robust solvers like PnP [19] with RANSAC [18]. Such methods achieve state-of-the-art (SOTA) results on visual localization benchmark but face limitations including inference speed, limiting their applicability to the real-world. The Scene Coordinate Regression (SCR) based method [6, 7, 25, 32, 50] does not involve creating the explicit map representation to establish correspondences but rather learns the implicit representation of the scene using neural networks and directly outputs the 2D-3D correspondences given a query image. However, these methods struggle to generalize and require huge per-scene training time along with ground-truth supervision of keypoints, making them challenging to employ at scale and in unknown environments.

For real-time applications, pose regression based methods are sought out where given a query image the learning-based model directly predicts the corresponding global camera pose in a common coordinate reference frame. Absolute Pose Regression (APR) based methods [8, 12, 22] first learn the implicit representation of the environment given geo-tagged reference images as supervision and then during inference output the suitable camera pose for a query image. This allows for high inference speed time, but they also suffer from per-scene training time limiting their generalization abilities and performance degradation [41].

Relative Pose Regression (RPR) methods, such as [3, 11, 16, 24], on the other hand, are trained on image pairs to predict the relative camera pose between the two images. For visual localization, during inference, one image is the query im-

age while another typically comes from the top-k retrieved geo-tagged reference images of the environment. The predicted relative poses are then utilized with ground-truth poses of the reference (or database) images to recover the absolute pose using methods like Umeyama alignment [48], motion-averaging module [16] and so on. Recently, [16, 24] has shown the generalizability and faster inference speed capabilities of such feed-forward RPR based methods when trained on a large-scale of data. Despite achieving state-of-the-art (SOTA) performance and inference speeds, Pose Regression methods often exhibit inferior performance compared to other paradigms. We attribute this limitation to a lack of global spatial awareness; by training on image pairs, these models merely approximate poses from pairwise relationships [2] rather than capturing the broader scene context. Furthermore, these techniques typically estimate relative camera poses without 3D-aware constraints, neglecting the geometric and structural consistency between pairs. This vulnerability is further exacerbated by a reliance on Visual Place Recognition (VPR) for reference view selection, where the retrieval of non-overlapping pairs lacking co-visibility leads to inaccurate pose estimates and reduced system robustness.

To address these limitations, we introduce **MultiLoc**, a novel large-scale trained relative pose regression (RPR) framework comprising two main components. The first is a multi-view guided pose regressor that aggregates holistic spatial cues from k reference images and their corresponding ground-truth camera poses in a single forward pass. Unlike existing RPR methods that rely solely on pairwise visual appearance, MultiLoc integrates multi-view inputs and poses to achieve superior spatial and geometric grounding. By incorporating reference poses directly into the regression phase, our model anchors the query image within a known 3D context, or what we refer as *3D sub-scene context*, providing highly accurate estimates for the camera pose estimation task. The second stage recovers the absolute scale of the predicted relative pose, ensuring globally consistent metric localization. Thus, MultiLoc contrasts sharply with existing RPR methods that estimate relative camera poses between each individual image pair for camera pose estimation and visual localization pipelines that only introduce reference poses in a post-hoc stage to combine with error prone pairwise relative estimates. Furthermore, we demonstrate the effectiveness of co-visibility aware input reference set rather than traditional visual place retrieval. Finally, we show the zero-shot capability of our proposed method, MultiLoc, by benchmarking multiple datasets for relative camera pose estimation and visual location tasks.

Therefore, the main contributions of this work are as follows:

1. We propose a new approach for relative pose regression methods that grounds a query image in 3D sub-scene context during the pose estimation itself.
2. We introduce MultiLoc, a two-stage visual re-localization method, that effectively integrates multi-view spatial and geometric cues from reference poses for accurate localization.
3. We investigate reference view selection issue and propose co-visibility-aware retrieval as a geometrically consistent alternative to traditional VPR, enhancing multi-view pose-guided regression robustness.

4. Experimental results show our method surpasses both the non-pose regression methods like feature matching and relative pose regression (RPR) methods on the relative camera pose estimation task. Meanwhile, MultiLoc achieves SOTA localization performance compared to RPR methods with high runtime efficiency.

2 Related Work

Relative camera pose estimation and visual re-localization tasks can both be solved by a common literature of work. Most of the literature fall under structure-based and structureless methods.

Structure-based Methods. These methods rely on establishing 2D-3D correspondences between a query image and the scene, typically through either explicit feature-matching [17, 38–40, 46, 52] or direct coordinate regression via neural networks [6, 7, 25, 32, 43, 50]. Following correspondence establishment, geometric algorithms such as PnP within a RANSAC loop are employed for robust pose estimation. While both feature-matching and scene coordinate regression (SCR) achieve high accuracy, their real-time application is often constrained by scene-specific training requirements, the need for extensive 3D representations, or high inference latency. Recent scene-agnostic coordinate regression methods [37, 47] alleviate the need for retraining; however, they often suffer from significant inference overhead—such as construction of cost volumes between query and multiple reference images or a continued dependency on sparse 2D-3D correspondences from Structure-from-Motion, limiting their suitability for real-time deployment.

Pose Regression Methods. Pose regression based methods, under structureless methods, do not involve establishing correspondences with the intermediate scene representation, rather the pose is directly predicted. When pose is predicted in a scene’s absolute or world coordinate frame as reference, it is called absolute pose regression (APR) [8, 12, 13, 22, 42] and when it is in reference to another image it is called relative pose regression (RPR) [3, 11, 16, 24, 54, 59]. Both of the methods can achieve real-time inference speed suitable for robotics applications. However, APR methods fall behind RPR methods in generalization abilities. Additionally, map-free approaches such as [2] act as a bridge between RPR and feature-matching methods. These works estimate the metric relative pose between a query and a single reference image by leveraging monocular depth and explicit feature matching; however, they remain dependent on known camera intrinsic parameters for accurate geometric back-projection. MultiLoc is also a RPR method, marking high performance and inference speed; therefore, most of our visual localization benchmark is with comparison to such methods.

3D Foundation Models. To enhance generalization across diverse environments, recent research has transitioned toward large-scale pre-training for 3D geometric representation learning. DUS3R [51], building upon the foundations of CroCo [53], pioneered this shift by employing a pointmap representation to establish dense, view-independent 2D-3D correspondences. This framework was further specialized for visual localization by ReLoc3r [16], which achieved

state-of-the-art results in relative pose regression through large-scale supervision. However, pairwise methods like DUSt3R often struggle with global consistency across multiple viewpoints. To address this, VGGT [49] introduced a unified transformer-based architecture capable of processing multiple images simultaneously, capturing superior geometric context compared to independent image pairs. Given that visual re-localization typically involves a query image and a set of reference frames, we propose to leverage a multi-view transformer architecture as [49] with pose prior for reference images. We hypothesize that joint processing of all available views along with camera poses of reference images facilitates a more holistic and better grounded understanding of spatial context, leading to more robust camera pose estimation and improved localization accuracy.

Co-visibility-aware retrieval. Co-visibility refers to the shared observation of 3D scene geometry across multiple viewpoints. In visual localization, the accuracy of camera pose estimation is inherently tied to the geometric consistency of the retrieved reference set. While structure-based methods leverage co-visibility via explicit 3D maps or incremental Structure-from-Motion [26, 34, 58], structureless approaches—particularly pose regressors—rarely exploit this geometric prior. Although AlligatOR [31] estimates co-visibility masks for relative pose estimation, integrating such priors into retrieval stage for pose regression remains under-explored. Significant progress was recently made by MegaLoc [5], that demonstrated co-visibility-aware training not only enhances visual place recognition but also directly improves downstream localization performance through superior image retrieval. In this work, we demonstrate that [5] features provide more geometrically relevant reference views, than traditional visual place recognition, that are critical for effective multi-view guidance of our model.

3 Method

Problem Statement. Given a database of k images, $\mathbf{I} = \{I_i\}_{i=1}^k$, $| I_i \in \mathbb{R}^{H \times W \times 3}$, from a scene with their absolute camera poses, $P = \{p_1, p_2, \dots, p_k\} | p_i \in \text{SE}(3)$, in a common world coordinate system, visual localization aims to find the absolute camera pose of a query image I_q .

Method Overview. We present MultiLoc, a robust relative pose regression framework designed for visual localization and camera pose estimation task. Unlike existing methods such as [16, 24], which operate on isolated image pairs, MultiLoc ingests a sequence of $(k + 1)$ images. By utilizing the first k relative camera poses as geometric priors along with the images, our model achieves a more comprehensive spatial understanding of the scene, leading to significantly enhanced relative camera pose estimation accuracy for the query frame..

3.1 Architecture

We begin by describing the architecture that is common for both camera pose estimation and visual re-localization. Input to our model at a time are $k+1$ images and k corresponding relative camera poses. The poses are input as members

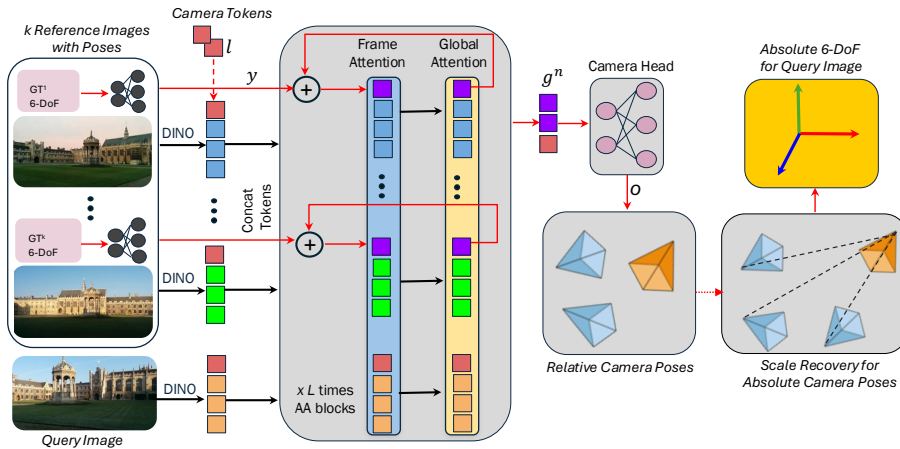


Fig. 2: MultiLoc Architecture overview. MultiLoc is a visual localization method where query poses are estimated using co-visible retrieved images with known camera poses. The retrieved images’ extrinsics are embedded via an MLP into camera tokens y and added with learnable camera tokens l , while all images pass through DINO-v2 [33] to obtain patch tokens. All the tokens are then concatenated and processed by alternating-attention (AA) transformer blocks. Finally, camera tokens are used to predict relative poses between query and reference images followed by geometric optimization for scale recovery and obtaining global pose for the query image. The red arrows denote the flow of camera tokens.

of $SE(3)$ manifold which are flattened to \mathbb{R}^{12} . A small multi-layer perceptron (MLP) is then applied to encode each of the camera pose as: $MLP : p_i \in \mathbb{R}^{12} \mapsto y_i \in \mathbb{R}^d$. The poses are normalized by the average distance, s , to camera centers with respect to the first frame as world coordinate frame: $s = \frac{1}{k} \sum_{i=1}^k \|c_i\|$ where c_i is the translation component of a camera pose.

The images, $I = \{I_1, \dots, I_k, I_q\}$, are tokenized in a patch of size 14 and fed into the DINO-v2 [33] model to obtain per-patch features $f \in \mathbb{R}^d$. Learnable camera tokens, $l = \{l_i\}_{i=1}^{k+1}$ are then added with ground-truth camera tokens, y , to form final pose tokens as: $g = l + y$. For the query image, we use $y_q = \mathbf{0} \in \mathbb{R}^d$. Finally, pose tokens are concatenated with register tokens, r and image patch tokens, f , to form the input to our transformer block as follows: $t = [g, r, f]$, where $[\cdot]$ is a concatenation operation.

Finally, our transformer model ingests all the tokens and first perform self (or frame) attention followed by cross (or global) attention across all the tokens t similar to [49]. This allows each token, especially query image tokens, to be grounded with scene’s 3D spatial context which pair-wise peers lag. The transformer block is repeated L times where after every frame attention we add the ground truth encoded pose tokens, y , for long-term context as $g^n = g^o + y$ where g^o is the output from previous layer and $g^o = g$ for the first transformer block.

Camera Pose Estimation. For camera pose estimation, the learnable camera tokens are sampled from the $L - th$ transformer block’s output and input into a simple four-layer self-attention-based camera head followed by a linear layer. The camera head predicts both the relative camera extrinsic and intrinsic parameters as:

$$C(\cdot) : g^n \mapsto o \in [q, c, f_x, f_y]$$

where q_i is the quaternion representation $\in \mathbb{R}^4$, $c_i \in \mathbb{R}^3$ is the translation component at a normalized scale and finally f_x and f_y are the focal lengths. Note that our method does not depend on camera intrinsics of input images but rather can predict it similar to [49]. In addition, the extrinsics, $q&c$, are relative to first image as the reference coordinate system.

3.2 Visual Re-Localization

So, far we have detailed the method to estimate the camera poses of the input images. For visual re-localization, we first retrieve the top-k most suitable images from the mapping set/dataset to the query image using a *co-visibility aware* retrieval method. This departs from the traditional visual localization pipeline that just utilizes visual place recognition (VPR)-based retrieval. Sec. 4 highlight that such a paradigm results in more robust performance than VPR. For co-visibility-awareness, we utilize the feature space of MegaLoc [5]. MegaLoc’s training enforces feature-space proximity for images sharing both geographic closeness and 3D surface overlap or co-visibility, ensuring that distance in the embedding space reflects a loss of visual overlap. This premise is different from other VPR methods that cater to geographic proximity. Consequently, this reference view selection strategy enables the model to prioritize images that provide more pertinent spatial context for the query.

Following retrieval, the tokens are created and processed as mentioned in Sec. 3.1 and finally the relative camera poses o is obtained. For localization, we just take the last token prediction from the camera head corresponding to the query image. However, the pose o_q or rather $o_{1,q}$, is at a normalized scale and in the co-ordinate frame of the first image.

Scale Recovery. To recover the scale and achieve a global pose for the query image in world coordinate frame, we perform geometric optimization. First, we compute the relative poses $\{o_{i,q}\}_{i=1}^k$ between the query and each database image. Then, for translation, the global scale is recovered by solving a least-squares problem that minimizes the squared distances between the reference camera centers and the back-projected translation rays of $o_{i,q}$, a process analogous to multi-view triangulation. The global rotation \hat{R}_q is then determined by computing the robust median of the calculated per-candidate orientations $\hat{R}_q = R_i \hat{R}_{i,q}$, where R_i is the rotation of the i -th reference image and $\hat{R}_{i,q}$ is the relative rotation between the query and i -th reference candidate. This is similar to the motion-averaging module as introduced in [16]. We also ablated various scale recovery techniques, such as Umeyama alignment [48] and motion averaging; results de-

tailed in the Appendix demonstrate that motion averaging yields the best overall performance. The full pipeline for MultiLoc is described in Fig. 2.

3.3 Training Details

We initialize MultiLoc’s weight with VGGT [49] and finetune on 4 H200s with a total of 1M iterations. Our model comprises of 1.1 billion parameters in total and is trained using AdamW optimizer with learning rate of 1×10^{-5} decaying to 1×10^{-8} and using bfloat 16 precision. The number of transformer blocks, comprising of frame and global attention, is $L = 24$. The aspect ratio of input images is randomized to be between 0.33 and 1, where the width is resized to be of maximum length as 518 pixels. Data augmentations and input image sampling is applied similar to [49]. For training we utilize Co3D [36], DL3DV [28], VKITTI2 [9], BlendedMVS [55], Re10K [60], MegaDepth [27] and ARKitScenes [4].

Loss function. For training we extend the homoscedastic uncertainty-based geometric loss function [21] to regress on both the camera extrinsic and intrinsic parameters as follows:

$$\text{loss}_x = |x^{\text{pred}} - x^{\text{gt}}| \quad (1)$$

$$\text{loss}(\cdot) = \sum_x \text{loss}_x \cdot e^{-s_x} + s_x \quad (2)$$

where x is a random variable being translation, rotation or focal length component and $s_x \in \{s_c, s_q, s_f\}$ are the learnable homoscedastic uncertainty scalar values for each of the x task variables respectively.

4 Experiment

Setup. Given that MultiLoc is a large-scale trained model, we evaluate its zero-shot generalization across diverse environments, including outdoor and natural domains. Our benchmarking focuses on two primary tasks: relative camera pose estimation and visual re-localization. For relative pose estimation, we report the Area Under the Curve (AUC@ θ), representing the percentage of image pairs with the maximum error between rotation and translation angles within θ . For visual re-localization, results are reported as translation error in meters (m) and rotation error in degrees ($^\circ$) unless otherwise specified.

Baselines. We evaluate our model primarily against state-of-the-art (SOTA) relative pose regression methods, reflecting our model’s underlying architecture. We benchmark against current leaders in this category, including ReLoc3r [16] and GeLoc3r [24]. As VGGT [49] processes multiple images together to estimate camera poses, it also serves as a robust baseline; we utilize VGGT’s direct pose predictions rather than inferring poses from reconstruction output for evaluation.

Table 1: Relative Camera Pose Estimation results on ACID and MegaDepth-1500. **Non-PR** denotes non-pose regression methods and **PR** Relative Pose Regression. VGGT-pair represents a pair of images as input while VGGT represents when the same number of images as MultiLoc is used. **Red** indicates best, **bold** second best.

Method		ACID (AUC@ θ \uparrow)			MegaDepth-1500 (AUC@ θ \uparrow)		
		5°	10°	20°	5°	10°	20°
Non-PR	Efficient LoFTR [52]	–	–	–	52.80	69.19	81.18
	ROMA [17]	46.30	58.80	68.90	62.60	76.70	86.30
	DUST3R [51]	21.50	35.95	49.70	27.90	46.00	63.30
	MASt3R [23]	52.12	64.54	73.61	42.40	61.50	76.90
	NoPoSplat [56]	48.60	61.70	72.80	–	–	–
PR	Map-free (SN) [2]	1.32	5.82	16.28	–	–	–
	Map-free (MF) [2]	2.57	9.96	24.50	–	–	–
	ExReNet (SN) [54]	1.90	7.53	18.69	–	–	–
	ExReNet (SUNCG) [54]	4.14	13.43	27.70	–	–	–
	ReLoc3r-224 [16]	28.25	47.34	62.54	39.90	59.70	75.40
	ReLoc3r-512 [16]	38.18	56.39	70.34	49.59	67.84	81.22
	VGGT-pair-518 [49]	22.59	40.83	59.04	40.93	60.81	76.61
	VGGT-518 [49]	25.58	44.47	62.20	46.25	66.46	80.71
	MultiLoc-518 (Ours)	72.24	84.22	91.52	68.42	81.16	89.34

4.1 Relative Camera Pose Estimation

Relative camera pose estimation aims at recovering the relative pose between images. We evaluate pairwise relative poses on the MegaDepth-1500 benchmark [44] and the Aerial Coastline Imagery Dataset (ACID) [29]. These datasets offer complementary challenges as MegaDepth consists of crowd-sourced Internet photos featuring diverse multi-view perspectives of outdoor landmarks, while ACID provides sequential drone footage of natural coastal scenes. As neither dataset was included in our training pipeline, these experiments serve to demonstrate the zero-shot generalization capabilities of MultiLoc. Following [16, 44, 56], we report the AUC@5/10/20. Since MultiLoc is trained to be guided by other views, in addition to a pair of image, we inject additional supporting 10 images that are randomly sampled per pair along with their relative camera poses. The AUC metric is computed only on the initial intended pair that was utilized by other models. Similarly, we also provide additional supporting images for the evaluation on VGGT.

MultiLoc’s pose regressor is not only able to achieve state-of-the-art (SOTA) results compared to relative pose regression, but also consistently surpasses feature matching and non-pose regression based methods as shown in Tab. 1. Our results highlight the importance of grounding the query image in the known 3D geometric context while regressing the pose.

4.2 Visual Re-Localization

Outdoor Visual Re-Localization. We evaluate MultiLoc’s visual re-localization performance on the Cambridge Landmarks [22] and WaySpots [6] benchmarks.

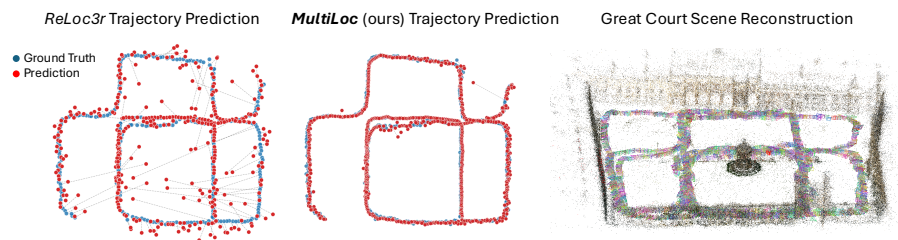


Fig. 3: MultiLoc v/s ReLoc3r trajectory error depiction on GreatCourt sequence of Cambridge dataset. Gray dashed lines indicate the translational error between **ground truth** and **predicted** poses. MultiLoc achieves significantly lower error by leveraging 3D sub-scene context from multiple images and their pose, whereas ReLoc3r’s reliance on pairwise images lead to higher drift.

The Cambridge Landmarks dataset provides diverse outdoor scenes characterized by significant environmental clutter and temporal variations in lighting and weather. On the other hand, WaySpots dataset, a subset of Niantic Map-Free [2], incorporates small outdoor places of interests like lawn, sign-boards or sculptures. Again, both of these datasets are entirely not seen by our model, and therefore we report the zero shot results from MultiLoc. We report the median rotation (in degrees) and median translation (in meters) errors for visual re-localization performance. Following [16], we retrieve the top-10 reference images per query for the regression-based baselines [16, 24] using Visual Place Recognition (VPR). For MultiLoc, we evaluate performance using both VPR-based and our proposed co-visibility-aware retrieval. Since our work advances structureless methods, we perform benchmarking that fall under such category. Tab. 2 and Tab. 3 shows the performance of various structureless and relative pose regression baseline methods on the Cambridge Landmarks [22] and WaySpots [6] dataset respectively. Our method significantly enhances visual localization performance, yielding improvements of around 41% and 37% on the Cambridge benchmark, and 67% and 63% on WaySpots benchmark for translation and rotation, respectively. These results underscore the importance of leveraging the 3D sub-scene context pre-emptively using multi-view and poses to mitigate uncertainty for accurate localization. The robustness of our method is also qualitatively validated by comparing its performance to the state-of-the-art ReLoc3r [16] framework, as shown in Fig. 3.

Indoor Visual Re-Localization. To further benchmark the cross-dataset transferability of our method, we conduct zero-shot evaluations on the Indoor6 [15] dataset. Unlike static benchmarks, Indoor6 introduces dynamic environmental factors, including day-night transitions and illumination changes across six diverse scenes. Tab. 4 highlights the efficacy of MultiLoc, where it achieves competitive SOTA performance, validating its ability to handle the geometric and photometric complexities of indoor scenes without prior fine-tuning.

Table 2: Visual Re-Localization benchmarking of methods on Cambridge dataset. Translation error is in meters (m) and median rotation error in degrees ($^{\circ}$).

Methods	GreatCourt	KingsCollege	OldHospital	ShopFacade	StMarysChurch	Average (4)	Average (\downarrow)
EssNet (7S) [59]	-	-	-	-	-	10.36/85.75	-
NC-EssNet (7S) [59]	-	-	-	-	-	7.98/24.35	-
ExReNet (SN) [54]	10.97/6.52	2.48/2.92	3.47/3.90	0.90/3.27	2.60/4.98	2.36/3.77	4.08/4.32
ExReNet (SUNCG) [54]	9.79/4.46	2.33/2.48	3.54/3.49	0.72/2.41	2.30/3.72	2.22/3.03	3.74/3.31
Map-free (Match) [2]	9.09/5.33	2.51/3.11	3.89/6.44	1.04/3.61	3.00/6.14	2.61/4.83	3.90/4.93
Map-free (Regress) [2]	8.40/4.56	2.44/2.54	3.73/5.23	0.97/3.17	2.91/5.10	2.51/4.01	3.69/4.12
ImageNet+NCM	-	-	-	-	-	0.83/1.36	-
ReLoc3r-224 [16]	1.71/0.94	0.47/0.41	0.87/0.66	0.18/0.53	0.41/0.73	0.48/0.58	0.73/0.65
ReLoc3r-512 [16]	1.22/0.73	0.42/0.36	0.62/0.55	0.13/0.58	0.34/0.58	0.38/0.52	0.55/0.56
GeLoc3r-512 [24]	1.07/0.52	0.41/0.34	0.64/0.54	0.15/0.64	0.27/0.58	0.37/0.53	0.51/0.52
MultiLoc-518 (ours)	0.44/0.21	0.34/0.33	0.41/0.48	0.09/0.31	0.23/0.34	0.27/0.365	0.302/0.334

Table 3: Visual Re-Localization benchmarking of methods on the WaySpots dataset as translation error (m)/ median rotation error ($^{\circ}$). We only report the top two performing relative pose regression models. For now, GeLoc3r’s [24] checkpoint is not available, so we did not benchmark it.

Methods	Bears	Cubes	Insc	Lawn	Map	SqB.	Statue	Tendrils	Rock	Wintersign	Average (\downarrow)
ReLoc3r	0.14/3.76	1.32/5.01	0.36/3.77	0.88/31.99	0.24/3.23	0.32/2.68	8.95/17.94	1.00/33.15	0.09/1.40	6.17/16.34	1.947/11.927
MultiLoc (ours)	0.062/1.85	0.30/2.39	0.17/2.83	0.36/10.75	0.12/1.37	0.23/1.44	2.20/4.83	0.97/13.58	0.08/1.25	1.90/2.93	0.639/4.322

Fig. 4 demonstrates the visual re-localization performance of MultiLoc on Indoor6 benchmark.

Table 4: Visual Re-Localization results on Indoor6 dataset. Median translation and rotation errors are reported as *cm* ($^{\circ}$). MultiLoc* signifies the frozen state of the pose regressor, which incorporates the pre-trained weights of the VGGT transformer and its associated camera head. **Red** denotes the best result.

Method	Scene1	Scene2a	Scene3	Scene4a	Scene5	Scene6	Avg <i>cm</i> ($^{\circ}$)
ReLoc3r	8.0 (0.60)	11.0 (0.78)	4.0 (0.44)	9.0 (0.87)	29.0 (1.60)	3.0 (0.52)	10.67 (0.80)
MultiLoc* (ours)	3.1 (0.54)	5.6 (0.49)	2.5 (0.52)	6.0 (0.61)	5.8 (0.66)	1.9 (0.53)	4.15 (0.56)
MultiLoc (ours)	2.6 (0.41)	4.2 (0.31)	2.3 (0.37)	4.7 (0.53)	5.7 (0.51)	1.8 (0.38)	3.5 (0.42)

4.3 Ablation Study

Co-visibility Aware Retrieval. We highlight the efficacy of our proposed co-visibility aware retrieval for robust visual localization in both quantitative and qualitative manner. For a fair comparison, we utilize DINO-SALAD [20] for VPR-based retrieval and MegaLoc [5] for co-visibility-based retrieval. MegaLoc is architecturally grounded in DINO-SALAD, sharing a nearly identical structure, yet it differs in its training paradigm. Specifically, while standard VPR models are typically trained on geographic proximity, MegaLoc is trained on a

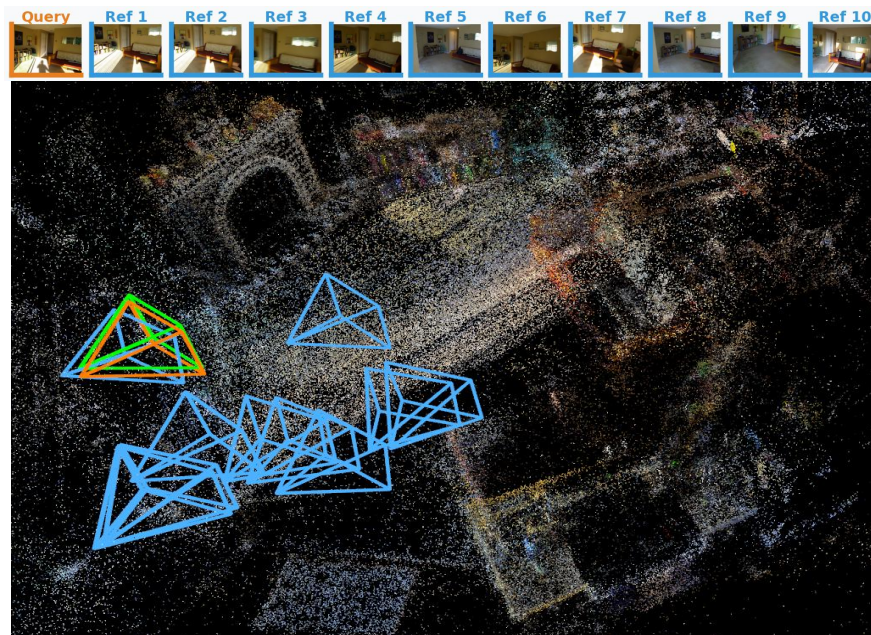


Fig. 4: Visual re-localization result on Indoor6 benchmark. Top row represents the **query** image and its corresponding retrieved **reference** views. Bottom represents the 3D reconstructed scene from Indoor6 dataset and the estimated camera pose for query image. MultiLoc achieves high re-localization accuracy for both translation and rotation components in indoor domain as demonstrated by **green** colored MultiLoc’s camera prediction closeness to **orange** colored ground truth query pose frustum. **Blue** frustums represent the supportive reference views.

multi-domain fusion including Structure-from-Motion (SfM) data. This allows it to leverage co-visibility constraints—mining tuples of images that share geometric overlap—rather than relying solely on coarse GPS-based nearby locations. We also employ NetVLAD [1] as a baseline for demonstrating the limitations of retrieving images with weak geometric overlap. As shown in Tab. 5, co-visibility-based retrieval consistently outperforms VPR on both the Cambridge and WaySpots benchmarks. This is largely because the former successfully retrieves reference images with high geometric overlap that is more suitable for pose estimation tasks, while VPR-based retrieval often converges on geographically similar but sparse co-visible regions. Tab. 5 also illustrates the advantage of our large-scale training paradigm. By conditioning the query image on scene context, by utilizing camera poses and retrieved images, our approach significantly outperforms frozen VGGT that rely solely on raw image inputs. Qualitatively, Fig. 5 specifically shows the statue structure from opposite viewpoints in the VPR-retrieved frames resulting in little-to-no co-visibility and poorly constrained relative pose estimation. However, the pose estimation is much less

Table 5: Median pose error [cm ($^\circ$)] comparison across MultiLoc’s states and retrieval methods on all 5 sequences of Cambridge and 10 for WaySpots dataset. ❄ denotes frozen (or just VGGT weights) and 🔥 denotes trained weights. Red highlights the best and blue for second best.

State	Retrieval	Cambridge (5)	WaySpots (10)
❄ Frozen	VPR (NetVLAD)	42.4 cm (0.374 $^\circ$)	134.1 cm (5.92 $^\circ$)
	VPR (SALAD)	37.0 cm (0.33 $^\circ$)	103.0 cm (5.85 $^\circ$)
	Covis.	35.2 cm (0.35 $^\circ$)	99.2 cm (4.82 $^\circ$)
🔥 Train	VPR (NetVLAD)	31.3 cm (0.34 $^\circ$)	75.2 cm (5.53 $^\circ$)
	VPR (SALAD)	31.8 cm (0.33 $^\circ$)	69.7 cm (5.32 $^\circ$)
	Covis.	30.2 cm (0.33 $^\circ$)	63.9 cm (4.32 $^\circ$)

erroneous when the retrieved frames have higher co-visibility with the query image.

Inference Speed Comparison. Real-time viability is essential for autonomous navigation tasks. Tab. 6 evaluates the inference throughput (FPS) and latency of our model on a NVIDIA H100 GPU using float32 datatype with Automatic Mixed Precision (AMP) for efficient speed and memory consumption without sacrificing the performance. To ensure a fair comparison with ReLoc3r, we select nearby resolutions that yield optimal performance for each architecture, accounting for differences in patch sizes. Notably, MultiLoc achieves an approximate 2 \times speedup over ReLoc3r; while the latter requires exhaustive pairwise processing, our model performs joint inference across the entire image sequence, made from query and reference set, in a single pass.

Table 6: Inference speed comparison. Latency (ms) and throughput (FPS) are measured for visual re-localization.

Resolution	ReLoc3r	MultiLoc (Ours)
512 ² vs. 518 ²	493.41 ms (2.03)	308.11 ms (3.25)
512 \times 384 vs. 518 \times 378	444.42 ms (2.25)	213.62 ms (4.68)

Effect of k for localization. Initially, we hypothesize a positive correlation between the density of reference set (k) and the resulting pose estimation accuracy. In this section, we analyze the impact of the retrieval parameter k —representing the number of reference images—on both localization accuracy and computational latency. As illustrated in Fig. 6, both translation and rotation error decreases as k increases; however, this gain comes at the cost of higher inference time. We observe that $k = 10$ provides an optimal balance for MultiLoc, delivering high-precision results while maintaining efficient real-time performance.



Fig. 5: Comparison of reference-view selection strategies. Compared to VPR-based retrieval (top), our co-visibility-based reference set (bottom) exhibits higher 3D surface overlap, or co-visibility, with the query. This geometric consistency and spatial relevance mitigate pose estimation errors, as evidenced by the shorter line length (purple dashed line) for positional error and closer alignment between ground truth and predicted viewing direction rays for rotation. In contrast, VPR-selected views suffer from poor 3D surface overlap, leading to higher angular and positional errors. Orange represents the GT query pose frustum, green for prediction and blue for reference views.

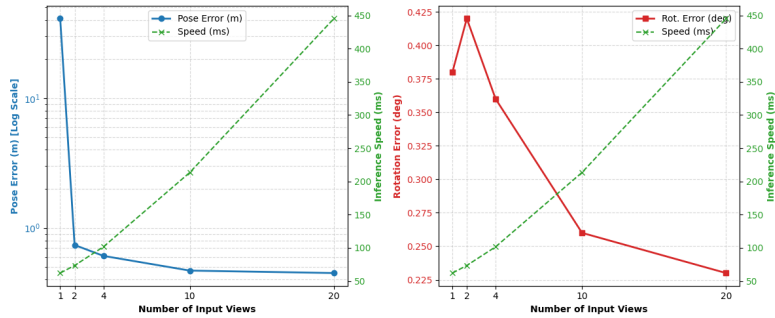


Fig. 6: Visual Localization performance and inference speed comparison across varying numbers of input views (k).

5 Conclusion

We present MultiLoc, a large-scale, multi-view guided pose regression model with zero-shot generalization. It is designed for robust pose estimation and visual re-localization across diverse indoor, outdoor, and natural environments. Our method jointly aggregates multiple reference views along with their respective camera poses that significantly reduces pose error and provides robust geometric grounding. Furthermore, we investigate the reference view selection problem and demonstrate that incorporating a co-visibility-aware retrieval mechanism

ensures high-quality reference selection suitable for our method’s robustness. Although our proposed methodology typically ensures co-visible reference set, we observe occasional retrieval failures that negatively impact pose estimation. This highlights the sensitivity of relative pose regression-based methods to retrieval quality and suggests a promising avenue for future investigation into robust reference view selection. Beyond accuracy, MultiLoc optimizes inference efficiency for visual localization; by processing multiple references in a single forward pass and bypassing the need for individual query-reference estimations. Our approach advances the state-of-the-art in relative camera pose regression, achieving substantial performance gains across visual localization and relative camera pose estimation benchmarks.

Acknowledgements

This work was supported by Clemson University’s Virtual Prototyping of Autonomy Enabled Ground Systems (VIPR-GS), under Cooperative Agreement W56HZV-21-2-0001 with the US Army DEVCOM Ground Vehicle Systems Center (GVSC).

References

1. Arandjelovic, R., Gronat, P., Torii, A., Pajdla, T., Sivic, J.: Netvlad: Cnn architecture for weakly supervised place recognition. In: Proceedings of the IEEE conference on computer vision and pattern recognition. pp. 5297–5307 (2016) [12](#)
2. Arnold, E., Wynn, J., Vicente, S., Garcia-Hernando, G., Monszpart, A., Prisacariu, V., Turmukhambetov, D., Brachmann, E.: Map-free visual relocalization: Metric pose relative to a single image. In: European Conference on Computer Vision. pp. 690–708. Springer (2022) [3](#), [4](#), [9](#), [10](#), [11](#)
3. Balntas, V., Li, S., Prisacariu, V.: Relocnet: Continuous metric learning relocalisation using neural nets. In: Proceedings of the European conference on computer vision (ECCV). pp. 751–767 (2018) [2](#), [4](#)
4. Baruch, G., Chen, Z., Dehghan, A., Dimry, T., Feigin, Y., Fu, P., Gebauer, T., Joffe, B., Kurz, D., Schwartz, A., et al.: Arkitscenes: A diverse real-world dataset for 3d indoor scene understanding using mobile rgb-d data. arXiv preprint arXiv:2111.08897 (2021) [8](#)
5. Berton, G., Masone, C.: Megaloc: One retrieval to place them all. In: Proceedings of the Computer Vision and Pattern Recognition Conference. pp. 2861–2867 (2025) [5](#), [7](#), [11](#), [22](#)
6. Brachmann, E., Cavallari, T., Prisacariu, V.A.: Accelerated coordinate encoding: Learning to relocalize in minutes using rgb and poses. In: Proceedings of the IEEE/CVF Conference on Computer Vision and Pattern Recognition. pp. 5044–5053 (2023) [2](#), [4](#), [9](#), [10](#)
7. Brachmann, E., Rother, C.: Visual camera re-localization from rgb and rgb-d images using dsac. IEEE transactions on pattern analysis and machine intelligence **44**(9), 5847–5865 (2021) [2](#), [4](#)
8. Brahmhatt, S., Gu, J., Kim, K., Hays, J., Kautz, J.: Geometry-aware learning of maps for camera localization. In: Proceedings of the IEEE conference on computer vision and pattern recognition. pp. 2616–2625 (2018) [2](#), [4](#)
9. Cabon, Y., Murray, N., Humenberger, M.: Virtual kitti 2. arXiv preprint arXiv:2001.10773 (2020) [8](#)
10. Castle, R., Klein, G., Murray, D.W.: Video-rate localization in multiple maps for wearable augmented reality. In: 2008 12th IEEE International Symposium on Wearable Computers. pp. 15–22. IEEE (2008) [2](#)
11. Chen, K., Snavely, N., Makadia, A.: Wide-baseline relative camera pose estimation with directional learning. In: Proceedings of the IEEE/CVF Conference on Computer Vision and Pattern Recognition. pp. 3258–3268 (2021) [2](#), [4](#)
12. Chen, S., Cavallari, T., Prisacariu, V.A., Brachmann, E.: Map-relative pose regression for visual re-localization. In: Proceedings of the IEEE/CVF Conference on Computer Vision and Pattern Recognition. pp. 20665–20674 (2024) [2](#), [4](#)
13. Chen, S., Wang, Z., Prisacariu, V.: Direct-posenet: Absolute pose regression with photometric consistency. In: 2021 International Conference on 3D Vision (3DV). pp. 1175–1185. IEEE (2021) [4](#)
14. Dai, A., Chang, A.X., Savva, M., Halber, M., Funkhouser, T., Nießner, M.: Scannet: Richly-annotated 3d reconstructions of indoor scenes. In: Proceedings of the IEEE conference on computer vision and pattern recognition. pp. 5828–5839 (2017) [21](#)
15. Do, T., Miksik, O., DeGol, J., Park, H.S., Sinha, S.N.: Learning to detect scene landmarks for camera localization. In: Proceedings of the IEEE/CVF Conference on Computer Vision and Pattern Recognition. pp. 11132–11142 (2022) [10](#)

16. Dong, S., Wang, S., Liu, S., Cai, L., Fan, Q., Kannala, J., Yang, Y.: Reloc3r: Large-scale training of relative camera pose regression for generalizable, fast, and accurate visual localization. In: Proceedings of the Computer Vision and Pattern Recognition Conference. pp. 16739–16752 (2025) [2](#), [3](#), [4](#), [5](#), [7](#), [8](#), [9](#), [10](#), [11](#), [21](#)
17. Edstedt, J., Sun, Q., Bökman, G., Wadenbäck, M., Felsberg, M.: Roma: Robust dense feature matching. In: Proceedings of the IEEE/CVF Conference on Computer Vision and Pattern Recognition. pp. 19790–19800 (2024) [4](#), [9](#)
18. Fischler, M.A., Bolles, R.C.: Random sample consensus: a paradigm for model fitting with applications to image analysis and automated cartography. Communications of the ACM **24**(6), 381–395 (1981) [2](#)
19. Gao, X.S., Hou, X.R., Tang, J., Cheng, H.F.: Complete solution classification for the perspective-three-point problem. IEEE transactions on pattern analysis and machine intelligence **25**(8), 930–943 (2003) [2](#)
20. Izquierdo, S., Civera, J.: Optimal transport aggregation for visual place recognition. In: Proceedings of the IEEE/CVF conference on computer vision and pattern recognition. pp. 17658–17668 (2024) [11](#)
21. Kendall, A., Gal, Y., Cipolla, R.: Multi-task learning using uncertainty to weigh losses for scene geometry and semantics. In: Proceedings of the IEEE conference on computer vision and pattern recognition. pp. 7482–7491 (2018) [8](#)
22. Kendall, A., Grimes, M., Cipolla, R.: Posenet: A convolutional network for real-time 6-dof camera relocalization. In: Proceedings of the IEEE international conference on computer vision. pp. 2938–2946 (2015) [2](#), [4](#), [9](#), [10](#)
23. Leroy, V., Cabon, Y., Revaud, J.: Grounding image matching in 3d with mast3r. In: European Conference on Computer Vision. pp. 71–91. Springer (2024) [9](#)
24. Li, J., Lee, Y., Fan, D.: Geloc3r: Enhancing relative camera pose regression with geometric consistency regularization. arXiv preprint arXiv:2509.23038 (2025) [2](#), [3](#), [4](#), [5](#), [8](#), [10](#), [11](#)
25. Li, X., Wang, S., Zhao, Y., Verbeek, J., Kannala, J.: Hierarchical scene coordinate classification and regression for visual localization. In: Proceedings of the IEEE/CVF Conference on Computer Vision and Pattern Recognition. pp. 11983–11992 (2020) [2](#), [4](#)
26. Li, Y., Snavely, N., Huttenlocher, D., Fua, P.: Worldwide pose estimation using 3d point clouds. In: European conference on computer vision. pp. 15–29. Springer (2012) [5](#)
27. Li, Z., Snavely, N.: Megadepth: Learning single-view depth prediction from internet photos. In: Proceedings of the IEEE conference on computer vision and pattern recognition. pp. 2041–2050 (2018) [8](#)
28. Ling, L., Sheng, Y., Tu, Z., Zhao, W., Xin, C., Wan, K., Yu, L., Guo, Q., Yu, Z., Lu, Y., et al.: D13dv-10k: A large-scale scene dataset for deep learning-based 3d vision. In: Proceedings of the IEEE/CVF Conference on Computer Vision and Pattern Recognition. pp. 22160–22169 (2024) [8](#)
29. Liu, A., Tucker, R., Jampani, V., Makadia, A., Snavely, N., Kanazawa, A.: Infinite nature: Perpetual view generation of natural scenes from a single image. In: Proceedings of the IEEE/CVF International Conference on Computer Vision. pp. 14458–14467 (2021) [9](#)
30. Liu, D., Cui, Y., Guo, X., Ding, W., Yang, B., Chen, Y.: Visual localization for autonomous driving: Mapping the accurate location in the city maze. In: 2020 25th international conference on pattern recognition (ICPR). pp. 3170–3177. IEEE (2021) [2](#)

31. Loiseau, T., Bourmaud, G., Lepetit, V.: Alligat0r: Pre-training through co-visibility segmentation for relative camera pose regression. arXiv preprint arXiv:2503.07561 (2025) [5](#)
32. Nguyen, S.T., Fontan, A., Milford, M., Fischer, T.: Focustune: Tuning visual localization through focus-guided sampling. In: Proceedings of the IEEE/CVF Winter Conference on Applications of Computer Vision. pp. 3606–3615 (2024) [2](#), [4](#)
33. Oquab, M., Darcet, T., Moutakanni, T., Vo, H., Szafraniec, M., Khalidov, V., Fernandez, P., Haziza, D., Massa, F., El-Nouby, A., et al.: Dinov2: Learning robust visual features without supervision. arXiv preprint arXiv:2304.07193 (2023) [6](#)
34. Panek, V., Kukulova, Z., Sattler, T.: Meshloc: Mesh-based visual localization. In: European Conference on Computer Vision. pp. 589–609. Springer (2022) [5](#)
35. Peng, H., Li, H., Dai, Y., Lan, Y., Luo, Y., Qi, T., Zhang, Z., Zhan, Y., Zhang, J., Xu, W., et al.: Omnivgg: Omni-modality driven visual geometry grounded transformer. arXiv preprint arXiv:2511.10560 (2025) [20](#)
36. Reizenstein, J., Shapovalov, R., Henzler, P., Sbordone, L., Labatut, P., Novotny, D.: Common objects in 3d: Large-scale learning and evaluation of real-life 3d category reconstruction. In: Proceedings of the IEEE/CVF international conference on computer vision. pp. 10901–10911 (2021) [8](#)
37. Revaud, J., Cabon, Y., Brégier, R., Lee, J., Weinzaepfel, P.: Sacreg: Scene-agnostic coordinate regression for visual localization. In: Proceedings of the IEEE/CVF Conference on Computer Vision and Pattern Recognition. pp. 688–698 (2024) [4](#)
38. Sarlin, P.E., Cadena, C., Siegwart, R., Dymczyk, M.: From coarse to fine: Robust hierarchical localization at large scale. In: Proceedings of the IEEE/CVF conference on computer vision and pattern recognition. pp. 12716–12725 (2019) [4](#)
39. Sarlin, P.E., Unagar, A., Larsson, M., Germain, H., Toft, C., Larsson, V., Pollefeys, M., Lepetit, V., Hammarstrand, L., Kahl, F., et al.: Back to the feature: Learning robust camera localization from pixels to pose. In: Proceedings of the IEEE/CVF conference on computer vision and pattern recognition. pp. 3247–3257 (2021) [2](#), [4](#)
40. Sattler, T., Leibe, B., Kobbelt, L.: Efficient & effective prioritized matching for large-scale image-based localization. IEEE transactions on pattern analysis and machine intelligence **39**(9), 1744–1756 (2016) [2](#), [4](#)
41. Sattler, T., Zhou, Q., Pollefeys, M., Leal-Taixe, L.: Understanding the limitations of cnn-based absolute camera pose regression. In: Proceedings of the IEEE/CVF conference on computer vision and pattern recognition. pp. 3302–3312 (2019) [2](#)
42. Shavit, Y., Ferens, R., Keller, Y.: Learning multi-scene absolute pose regression with transformers. In: Proceedings of the IEEE/CVF International Conference on Computer Vision. pp. 2733–2742 (2021) [4](#)
43. Shotton, J., Glocker, B., Zach, C., Izadi, S., Criminisi, A., Fitzgibbon, A.: Scene coordinate regression forests for camera relocalization in rgb-d images. In: Proceedings of the IEEE conference on computer vision and pattern recognition. pp. 2930–2937 (2013) [4](#)
44. Sun, J., Shen, Z., Wang, Y., Bao, H., Zhou, X.: Loftr: Detector-free local feature matching with transformers. In: Proceedings of the IEEE/CVF conference on computer vision and pattern recognition. pp. 8922–8931 (2021) [9](#)
45. Suomela, L., Kalliola, J., Dag, A., Edelman, H., Kämäräinen, J.K.: Benchmarking visual localization for autonomous navigation. In: Proceedings of the IEEE/CVF Winter Conference on Applications of Computer Vision. pp. 2945–2955 (2023) [2](#)
46. Taira, H., Okutomi, M., Sattler, T., Cimpoi, M., Pollefeys, M., Sivic, J., Pajdla, T., Torii, A.: Inloc: Indoor visual localization with dense matching and view synthesis. In: Proceedings of the IEEE conference on computer vision and pattern recognition. pp. 7199–7209 (2018) [2](#), [4](#)

47. Tang, S., Tang, C., Huang, R., Zhu, S., Tan, P.: Learning camera localization via dense scene matching. In: Proceedings of the IEEE/CVF Conference on Computer Vision and Pattern Recognition. pp. 1831–1841 (2021) [4](#)
48. Umeyama, S.: Least-squares estimation of transformation parameters between two point patterns. *IEEE Transactions on pattern analysis and machine intelligence* **13**(4), 376–380 (2002) [3](#), [7](#), [21](#)
49. Wang, J., Chen, M., Karaev, N., Vedaldi, A., Rupprecht, C., Novotny, D.: Vggt: Visual geometry grounded transformer. In: Proceedings of the Computer Vision and Pattern Recognition Conference. pp. 5294–5306 (2025) [5](#), [6](#), [7](#), [8](#), [9](#), [21](#)
50. Wang, S., Laskar, Z., Melekhov, I., Li, X., Zhao, Y., Toliás, G., Kannala, J.: Hscnet++: Hierarchical scene coordinate classification and regression for visual localization with transformer. *International Journal of Computer Vision* **132**(7), 2530–2550 (2024) [2](#), [4](#)
51. Wang, S., Leroy, V., Cabon, Y., Chidlovskii, B., Revaud, J.: Dust3r: Geometric 3d vision made easy. In: Proceedings of the IEEE/CVF Conference on Computer Vision and Pattern Recognition. pp. 20697–20709 (2024) [4](#), [9](#)
52. Wang, Y., He, X., Peng, S., Tan, D., Zhou, X.: Efficient loftr: Semi-dense local feature matching with sparse-like speed. In: Proceedings of the IEEE/CVF conference on computer vision and pattern recognition. pp. 21666–21675 (2024) [4](#), [9](#)
53. Weinzaepfel, P., Lucas, T., Leroy, V., Cabon, Y., Arora, V., Brégier, R., Csurka, G., Antsfeld, L., Chidlovskii, B., Revaud, J.: Croco v2: Improved cross-view completion pre-training for stereo matching and optical flow. In: Proceedings of the IEEE/CVF International Conference on Computer Vision. pp. 17969–17980 (2023) [4](#)
54. Winkelbauer, D., Denninger, M., Triebel, R.: Learning to localize in new environments from synthetic training data. In: 2021 IEEE International Conference on Robotics and Automation (ICRA). pp. 5840–5846. IEEE (2021) [4](#), [9](#), [11](#)
55. Yao, Y., Luo, Z., Li, S., Zhang, J., Ren, Y., Zhou, L., Fang, T., Quan, L.: Blended-mvs: A large-scale dataset for generalized multi-view stereo networks. In: Proceedings of the IEEE/CVF conference on computer vision and pattern recognition. pp. 1790–1799 (2020) [8](#)
56. Ye, B., Liu, S., Xu, H., Li, X., Pollefeys, M., Yang, M.H., Peng, S.: No pose, no problem: Surprisingly simple 3d gaussian splats from sparse unposed images. *arXiv preprint arXiv:2410.24207* (2024) [9](#)
57. Yeshwanth, C., Liu, Y.C., Nießner, M., Dai, A.: Scannet++: A high-fidelity dataset of 3d indoor scenes. In: Proceedings of the IEEE/CVF International Conference on Computer Vision. pp. 12–22 (2023) [20](#), [21](#)
58. Zeisl, B., Sattler, T., Pollefeys, M.: Camera pose voting for large-scale image-based localization. In: Proceedings of the IEEE International Conference on Computer Vision. pp. 2704–2712 (2015) [5](#)
59. Zhou, Q., Sattler, T., Pollefeys, M., Leal-Taixe, L.: To learn or not to learn: Visual localization from essential matrices. In: 2020 IEEE International Conference on Robotics and Automation (ICRA). pp. 3319–3326. IEEE (2020) [4](#), [11](#)
60. Zhou, T., Tucker, R., Flynn, J., Fyffe, G., Snavely, N.: Stereo magnification: Learning view synthesis using multiplane images. *arXiv preprint arXiv:1805.09817* (2018) [8](#)

Appendix

A Additional Training Configuration

A.1 Architecture Ablation

MultiLoc’s pose regressor employs learnable camera tokens for both reference and query images. While providing learnable tokens for images with known ground truth poses may initially appear redundant, empirical evidence suggests that utilizing a collective set of learnable tokens, l , significantly enhances training stability. As illustrated in Fig. 7, restricting learnable tokens to the query image alone (i.e., last learnable token) induces volatile gradient spikes, whereas our ‘all-learnable’ configuration facilitates smoother convergence. A similar holistic token learning design is also employed in concurrent work [35], which also reports reduced error when learnable tokens and ground-truth poses are used together. Due to the high computational overhead of full-scale training and availability of limited compute, these architectural ablations were initially conducted on the ScanNet++ [57] dataset as a representative for our broader multi-dataset training.

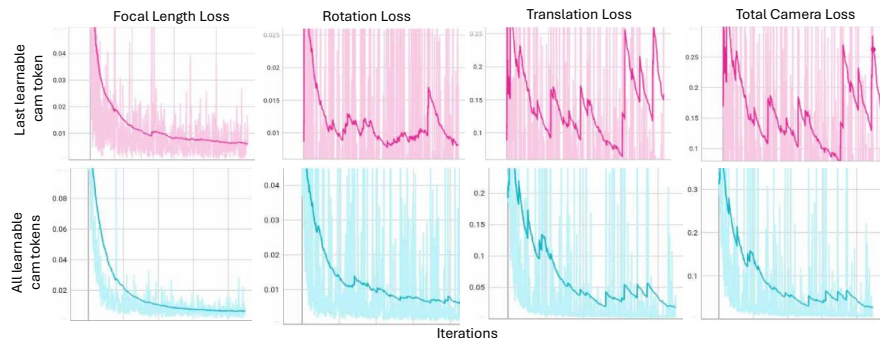


Fig. 7: Ablation study for MultiLoc’s architecture. Using learnable camera token only for the last image (top) leads to unstable training and sudden gradient jumps. Whereas, using learnable tokens for all the images in a sequence (bottom) and regressing upon them reduces this instability.

B More Experiments

In this section, we show the generalizability of our proposed model MultiLoc and its pose regressor on the indoor domain for both relative camera pose estimation and visual re-localization tasks.

Table 7: Relative camera pose estimation results on ScanNet-1500 dataset. **Red** indicates best, **bold** second best. While certain baseline results are cited from [16], we performed an independent benchmarking of our primary baselines, ReLoc3r and VGGT, within our own evaluation framework to ensure a consistent comparison.

Method		ScanNet-1500 (AUC@ θ \uparrow)		
		5°	10°	20°
Non-PR	Efficient LoFTR	19.20	37.00	53.60
	ROMA	28.90	50.40	68.30
	DUSt3R	23.81	45.91	65.57
	MASt3R	28.01	50.24	68.83
	NoPoSplat	31.80	53.80	71.70
	PR	Map-free (Regress-SN)	1.84	8.75
	Map-free (Regress-MF)	0.50	3.48	13.15
	ExReNet (SN)	2.30	10.71	26.13
	ExReNet (SUNCG)	1.61	7.00	18.03
	ReLoc3r-224 (Ours)	28.34	52.60	71.56
	ReLoc3r-512 (Ours)	34.78	58.31	75.52
	VGGT-518	38.93	60.49	76.56
	MultiLoc-518 (Ours)	55.63	72.90	83.82

B.1 Relative Camera Pose Estimation

We first evaluate the zero-shot generalization of our proposed model on the ScanNet-1500 benchmark for pairwise relative camera pose estimation. ScanNet-1500, a widely utilized subset of the ScanNet [14] indoor dataset. Notably, while the state-of-the-art ReLoc3r [16] is explicitly trained on the high-fidelity ScanNet++ [57] corpus, MultiLoc does not include any ScanNet-derived data in its training set. Consequently, this evaluation represents a completely unseen environment for our model. For our evaluation, we not only benchmark MultiLoc against ReLoc3r, a pairwise relative model, and VGGT [49], a multi-view input baselines but also feature matching and other relevant non-pose regression methods. Both MultiLoc and VGGT are fed the same number of images, and evaluation is conducted similarly to what was previously suggested. The SOTA results achieved by MultiLoc are highlighted in Tab. 7.

C Additional Ablation Study

C.1 Scale Recovery

We highlight the scale recovery of our relative camera poses using two methodologies. The first is a solution to the Procrustes Analysis; Umeyama Alignment [48], and second one is a motion averaging module that was suggested in [16]. For the former, to resolve the scale and gauge ambiguity between our model’s relative predictions and the global coordinate system, we perform a 7-DoF similarity alignment using the k reference frames. We utilize the Umeyama algorithm to compute a transformation $S \in \text{Sim}(3)$ that maps the local relative coordinate

frame to the metric world space. This transformation is then applied to the query pose to obtain its final global representation. For each scene, we report the rotation error because the difference between the two methods was found to be more significant than the translation component. Tab. 8 shows the motion averaging, as discussed in the main section, achieves a better result than Umeyama alignment.

Table 8: Scale Recovery benchmark of MultiLoc (ours) on Cambridge dataset for visual re-localization. Translation error is in meters (m) and median rotation error in degrees ($^{\circ}$).

Methods	GreatCrt	KingsClg	OldHosp	ShopFac	StMarys	Avg Rot ($^{\circ}$ ↓)	Avg Trans. (m↓)
Umeyama Align	0.32	0.47	0.73	0.36	0.49	0.48	0.30
Motion Avg	0.21	0.33	0.48	0.31	0.34	0.33	0.30

C.2 Failure Cases of Co-visibility-aware Retrieval

MultiLoc leverages co-visibility-aware retrieval for reference view selection, employing features from MegaLoc [5]. In this section, we demonstrate few failure case instances where the current co-visibility-aware retrieval mechanism proves insufficient, resulting in significant pose estimation errors, as illustrated in Fig. 8. One of the interesting scenarios from Fig. 8 highlights the street viewing direction that fails to successfully retrieve reference images. Exact scenarios where MegaLoc’s performance is suboptimal is mentioned in [5]. In contrast, our approach prioritizes geometric relevance for reference view selection; we demonstrate that, for feed-forward foundation models, the co-visibility criterion is more critical for optimal performance than traditional place recognition. Given the rapid advancements in feed-forward 3D geometry models, optimizing reference view selection with co-visibility criterion remains a critical challenge, which we designate for future works.



Fig. 8: Co-visibility-aware retrieval failure cases. The following cases illustrate scenarios where co-visibility-based retrieval features fail to identify appropriate reference images. We demonstrate using top-5 of 10 such reference images per query. Such instances result in significant translation (purple dashed line) and rotation errors between the ground truth and predicted camera poses.